corrosion and materials degradation

MDPI

Article

Influence of Silica Fume (SF) Content on Passive Film Formation of Steel Reinforcement Inside Hardened Concrete

Marcella Amaral, Isaac Aguiar Oliveira, Diogo Henrique de Bem, Giovana Costa Réus, Gustavo Macioski, Marcelo Miranda Farias and Marcelo Henrique Farias de Medeiros *

Center for Studies in Civil Engineering (CESEC), Department of Civil Engineering, Federal University of Paraná, Curitiba 81531-980, PR, Brazil; marcellamarp@gmail.com (M.A.); acaguiar@gmail.com (I.A.O.); diogobem@yahoo.com.br (D.H.d.B.); giovanacostareus@gmail.com (G.C.R.); gmacioski@gmail.com (G.M.); mirandafariasmarcelo@gmail.com (M.M.F.)

* Correspondence: marcelo.medeiros@ufpr.br; Tel.: +55-413361-3438

Abstract: Corrosion is one of the causes of failure in reinforced concrete structures, and forming a passive film on the steel is essential for protection. Although several studies have looked at passive film formation in concrete pore solutions, few have considered its formation in hardened concrete and the influence of silica fume (SF) in the binder composition. This study aims to evaluate the influence of the SF content on passive film formation time in concrete. Periodic measurements assessed the electrical resistivity and corrosion current density of concrete samples containing 5%, 10%, 15%, and 20% SF. The alkalinity of the mixtures and the kinetics of the pozzolanic reaction were also monitored by XRD and titration tests. The control mixtures exhibited susceptibility to corrosion, regardless of the curing age evaluated. In contrast, the partial replacement of cement with SF accelerated the formation of the passive film on the steel surface, suggesting a delayed onset of corrosion due to modifications in the physical properties of the concrete. Also, the portlandite content and pH can predict passive film formation, with SF significantly accelerating this process.

Keywords: silica fume; passive film formation; corrosion current density; electrical resistivity; portlandite content

Academic Editors: Igor Chaves, Robert B. Petersen and Robert Melchers

Received: 14 November 2024
Revised: 18 December 2024
Accepted: 7 January 2025
Published: 13 January 2025

Citation: Amaral, M.; Aguiar Oliveira, I.; de Bem, D.H.; Costa Réus, G.; Macioski, G.; Miranda Farias, M.; Farias de Medeiros, M.H. Influence of Silica Fume (SF) Content on Passive Film Formation of Steel Reinforcement Inside Hardened Concrete. *Corros. Mater. Degrad.* **2025**, *6*, 3. https://doi.org/10.3390/cmd6010003

1. Introduction

Corrosion is the primary failure mechanism in reinforced concrete structures [1–3]. Currently, especially as a result of climate change, the corrosion process is occurring at an accelerated rate [4,5]. Studies have shown that increasing the ambient temperature accelerates the diffusion of chlorides, with a direct impact on corrosion [5]. The same effect occurs with carbonation [6]. In this context, the passive film is the main form of protection of the steel rebar against it. It consists of a thin layer formed on the steel's surface under an alkaline environment (pH > 12.5), which has a high ohmic resistivity and negligible corrosion rate. Its formation is a dissolution–precipitation process, which consists of the dissolution of metallic cations in the alkaline solution and the precipitation of oxides/hydroxides on the metal surface [7].

The passive film has a layered structure, with an inner layer that forms and completely covers the metal. It then grows until it reaches a steady state that ensures full passivation [8]. According to Mudra et al. [9] and Williamson and Isgor [10], its thickness is directly proportional to the alkalinity of the medium. The precipitation of Fe oxides/hydroxides becomes harder in lower-pH media (pH < 11.5) due to the diluted OH^- ions, which

promote the solubility of Fe species at the film/solution interface [11,12]. Thus, an increased concentration of OH^- in the pore solution of reinforced concrete structures results in a lower probability of corrosion and a higher degree of rebar passivation.

The passivation time is an important item of information regarding the durability of concrete structures exposed to severe environments, since the passive film is the main protection against steel rebars' corrosion and structure failure. Many authors have studied this parameter using bars immersed in synthetic concrete/mortar pore solutions, as shown in Table 1. However, the passive film formation in solution does not indicate the real-time passivation in hardened cementitious materials, requiring more time to stabilize in the latter [7,13]. Nevertheless, researchers rarely use hardened concrete or mortar to estimate the time required for the formation of this protective layer. Only Ortolan, Mancio, and Tutikian [14] have used silica fume (SF) in a binder composition.

Table 1. Studies about the formation time for the passivation film of steel.

Paper	Saturated Calcium Hydroxide Solution	Concrete/Mortar Pore Solution	Hardened Concrete/Mortar
[15]	X		
[10,16]	X	X	
[9,17–24]		X	
[7]		X	X
[14,25,26], Present Study			X

Note: Database: Science Direct; Search Words: "passive film formation" AND "concrete" AND ("calcium hydroxide solution" OR "Concrete pore solution" OR "Mortar pore solution" OR "hardened concrete" OR "hardened mortar"); Period: 2015 to 2024.

According to Poursaee and Hansson [13], despite the high alkalinity of Portland cement composites, the passivation of reinforcing steel is not an instantaneous process; it requires at least 7 days for its complete formation in mortars with a water/cement (w/c) ratio of 0.45. This time increases when steel is inside concrete samples with a 0.50 w/c ratio, varying from 20 to 80 days [7,25]. Moreover, the time of rebar passivation in concrete increases with the decrease in the w/c ratio. Fan et al. [26] verified, through linear polarization resistance (LPR), that ultra-high-performance concretes (UHPCs) with a w/c ratio approximately equal to 0.16 and different contents of lightweight sand reached the low corrosion level zone between 20 and 120 days when considering B = 52 mV, where B is the Stern–Geary constant, used in LPR to calculate the corrosion current density. However, none entered the passivity zone (i_{corr} < 0.1 $\mu A/cm^2$) after 147 days of analysis. When combining the LPR and Tafel polarization test for each composition, the rebars were in the passive state in all UHPC samples throughout the test period of 147 days.

Despite the increase in mechanical strength, improvement of transport properties, and electrochemical behavior, concrete incorporating SF has a lower cement content due to its partial substitution and, consequently, promotes a less alkaline environment [27] and a more sustainable mixture [28]. The pozzolanic activity decreases the availability of calcium hydroxide, favoring a reduction in the pore solution alkalinity, which affects passivation layer formation on steel in reinforced concrete [29].

Yet, contrary to expectations, Ortolan, Mancio, and Tutikian [14] observed, through polarization resistance (Rp), that steel achieved the negligible zone of corrosion first in concrete with a w/c equal to 0.65 and partial replacement of cement by 5 and 10% of SF when compared with those without it, even though the OH^- concentration and pH were reduced. These authors verified the formation of a passive film after 3 days for concretes with 10% of SF, whereas in the control mix, passivation of the steel reinforcement

occurred only after 28 days. Oliveira and Cascudo [30] also showed that concrete with partial replacement of cement by SF presented electric resistivity corresponding to the zone of negligible probability of corrosion after 91 days of curing, whereas concrete samples without SF remained in the zone of moderate probability of corrosion after 650 days. This was reflected in a denser and more compact microstructure of concrete with SF, as well as a pore solution with lower conductivity, indicating the higher potential of durability of steel rebars due to the increased difficulty in the initiation and propagation of corrosion.

Despite the many research projects regarding passive film formation in synthetic solutions, which can simulate the presence of pozzolanic additions, no one has shown the influence of SF content on time for passive film formation using steel rebars embedded in hardened concrete. This study aimed to evaluate the passivation time of steel rebar, through electrochemical tests, inside a concrete sample containing SF as a partial replacement for cement at 5, 10, 15, and 20% (by weight). The electrochemical (current density and electrical resistivity) and chemical analyses (pH and XRD) support the discussions of the necessary time for passive film formation in steel rebars inside hardened concrete during 105 days of aging. The hypothesis raised is that, despite the decrease in pH due to pozzolanic reactions, using SF as a partial replacement of cement would improve the time of steel's passive film formation in hardened concrete samples, and the higher the content, the faster its formation. Thus, the combined analysis proposed here makes it possible to state the optimum content of SF for concrete structures regarding steel rebar protection against corrosion.

2. Materials and Methods

2.1. Materials

The experimental study consisted of casting reinforced concrete samples for electrochemical tests and cement pastes for chemical analysis. The binder in both mixtures resulted from combining commercial cement and silica fume in varying proportions.

CPV-ARI cement, equivalent to type III cement [31], was chosen because it has the lowest mineral addition content (<10%), allowing for a clearer analysis of the influence of substituting cement with SF. Table 2 shows the physical characteristics of this cement provided by the cement producer. The company Tecnosil (Campinas, Brazil) provided the silica fume. Table 3 shows the chemical composition of both binding materials obtained by X-ray fluorescence spectrometry. The fine fraction of the materials (<0.075 mm) was analyzed using a Shimadzu EDX-720 energy-dispersive X-ray fluorescence spectrometer.

Table 2. Characterization of Portland cement.

Fineness		Setting Time		Compressive Strength (MPa)				Chemical Requirements (%)	
Blaine (cm^2/g)	#200 (%)	Start (min)	End (min)	1 Day	3 Days	7 Days	28 Days	Insoluble Residue	Loss in Ignition (%)
4710	0.3	250	310	22.2	37.1	41.5	49.2	0.40	3.20

Table 3. X-ray fluorescence of Portland cement and silica fume (wt.%).

Sample	Chemical Composition (%)								
	CaO	SiO_2	Al_2O_3	SO_3	Fe_2O_3	MgO	K_2O	TiO_2	Na_2O_5
CPV-ARI	62.75	19.2	4.19	3.04	2.85	2.54	1.68	0.17	0.05
SF	0.51	92.49	1.91	2.08	0.13	-	2.76	-	-

The specific mass (1.95 g/cm^3) was determined according to the Le Chatelier method. The specific area (20.238 m^2/kg) was obtained using the liquid N_2 adsorption technique via Micromeritics Gemini 2380 equipment. The loss on ignition (2.70%) was determined in

a muffle furnace at 1000 °C. The modified Chapelle test was performed to investigate the SF pozzolanic activity by NBR 15895 [32]. The result, obtained by titration and expressed by the amount of calcium hydroxide fixed per gram of mineral addition, was 1542 mg $Ca(OH)_2$/g of SF. This value is 253% higher than the limit indicated by Raverdy et al. [33] as a characteristic of a pozzolanic material (436 mg $Ca(OH)_2$/g of pozzolan), confirming the high reactivity of the SF used in this study.

The aggregates for concrete samples were natural quartz sand with a fineness module of 2.24 and a specific mass of 2.62 g/cm^3 and basaltic gravel with a maximum diameter of 12.5 mm and a specific mass of 2.88 g/cm^3. A third-generation polycarboxylate-based superplasticizer additive was also used, with a specific mass of 1.10 ± 0.02 g/cm^3 and a recommended dosage of 0.3 to 2.0% of the weight of cement, as informed by the producer.

Gerdau's carbon steel bars (Curitiba, Brazil) with an 8 mm diameter, 500 MPa yield stress, 550 MPa tensile strength, and a minimum elongation of 8% in bars with a 10 mm diameter [34] were used as reinforcement in the concrete samples.

2.2. Sample Mixing, Casting, and Preparation

The mixing proportions of the concrete samples included partial cement replacement by SF with contents of 5, 10, 15, and 20% by weight (Table 4). The water/binder ratio (w/b) was kept constant, and the superplasticizer additive was used to achieve a 100 ± 20 mm slump value.

Table 4. Concrete mixing proportion.

Mix	Binder	Cement (kg)	Silica Fume (kg)	Sand (kg)	Gravel (kg)	w/b	Additive *
Control mix	1.0	1.00	0.00	3.05	3.74	0.58	-
SF-5%	1.0	0.95	0.05	3.05	3.74	0.58	0.30%
SF-10%	1.0	0.90	0.10	3.05	3.74	0.58	0.32%
SF-15%	1.0	0.85	0.15	3.05	3.74	0.58	0.32%
SF-20%	1.0	0.80	0.20	3.05	3.74	0.58	0.35%

* Superplasticizer in relation to cement weight.

The concrete samples consisted of 3 cylinders with dimensions of Ø10 × 20 cm to determine the compressive strength at 28 days, according to NBR 5739 [35].

Two prismatic samples (25 × 25 × 7 cm^3) of reinforced concrete were cast for each mix to evaluate the formation of the passive film through electrochemical techniques. The concrete was cast in one layer and vibrated on a 50 × 50 cm vibrating table for 20 s. Two steel bars were positioned in each sample, with a 3.1 cm cover (Figure 1). In these samples, the portion of the steel bars not embedded in concrete was coated with epoxy to prevent corrosion. Since each specimen had two steel bars, the electrochemical evaluation was based on four values per sample (two measurements per bar), performed at hydration ages of 14, 38, 55, 69, and 105 days.

Finally, cement pastes, with the same SF contents and w/b ratios, were prepared to evaluate the consumption and formation of hydrated compounds, as well as the pH of the mix. The mixing procedure of cement pastes followed the recommendations of NBR NM 5739 [35], and cylindrical samples (Ø10 × 20 mm) were cast, with three samples per group.

All samples (concrete, reinforced concrete, and cement paste) were cured in a humid chamber with humidity above 95% and a temperature of 22 ± 2 °C until the age of analysis.

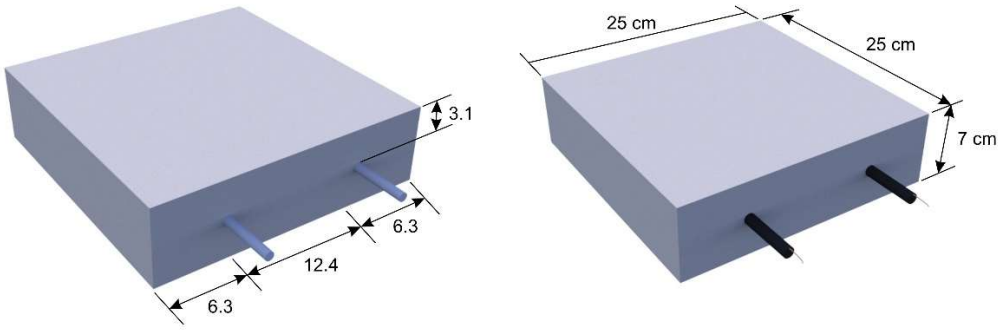

Figure 1. Dimensions of prismatic sample of reinforced concrete for electrochemical evaluation.

To conduct the tests on the cement pastes, hydration was suspended at the specified ages by immersing the small cement paste pieces in acetone P.A., followed by drying in an oven at 40 ± 5 °C until constant mass. The procedure adopted was based on Neithalath et al.'s [36] work and the criticism provided by Hoppe Filho et al. [37] regarding the temperature of drying used by the former (105 °C). Therefore, in the present study, the drying temperature was modified to prevent the desaturation, gel water desorption, and partial dehydration of the hydrated products of the cement pastes. To evaluate the kinetics of the hydration products and silica fume, tests were performed between 28 and 105 days.

2.3. Electrochemical Monitoring

The electrical resistivity test was performed on reinforced concrete samples using the four-point method (the Wenner method). Measurements were taken at the center of the samples, with the equipment positioned parallel to the steel bars, thus avoiding interference between the metallic elements.

Corrosion was evaluated using the linear polarization resistance (LPR) method with the modulated confinement of current (MCC) technique. The equipment employed was a Gecor 10 field potentiostat from GEOCISA (Madrid, Spain), which uses the linear polarization resistance technique to determine the corrosion current density (i_{corr}), as indicated by Equation (1). Table 5, in turn, was used as a reference for classifying the results of electrical resistivity and i_{corr} [38].

$$i_{corr} = \frac{B}{R_P} \quad (1)$$

where B is the Stern–Geary constant, with a value equal to 52 mV, and R_p is the linear polarization resistance, in kΩ × m^2.

Table 5. Parameters for analysis of the possibility or level of corrosion of rebar in concrete samples [35].

Resistivity (kΩ.cm)	Possibility/Corrosion Level	i_{corr} (μA/cm^2)
<10	High	>1.0
10–50	Moderate	1.0–0.5
50–100	Low	0.5–0.1
>100	Negligible	<0.1

It is worth mentioning regarding the corrosion rate that there is a zone of uncertainty between i_{corr} values of 0.1 (negligible corrosion) and 0.2 μA/cm^2 (low active corrosion level) [39]. Therefore, some authors have stated that only an i_{corr} > (0.1–0.2) should be considered as a risk to the durability of reinforced concrete [40]. Andrade and Alonso [38] reaffirm that i_{corr} values below 0.1 μA/cm^2 indicate negligible corrosion, so that passive film in the reinforcement rebar can be considered in a steady state.

The 0.1 to 0.2 μA/cm^2 range is a transition zone between the passive and active corrosion states. Due to the factor-2 error inherent in the Stern–Geary formula, which results from uncertainties in corrosion parameters [41], a value of 0.2 μA/cm^2 can be interpreted as equivalent to 0.1 μA/cm^2. For this reason, it is recommended to use 0.2 μA/cm^2 as the limit for depassivation. Thus, many authors consider that readings within this range indicate that the steel remains in a passive state, without significant active corrosion [13,14]. Based on the information presented in this paper, only i_{corr} values above 0.2 μA/cm^2 were considered as indicative of active corrosion in terms of application in reinforced concrete.

2.4. Monitoring of Hydration Kinetics

Hydration kinetics assessment was performed with X-ray diffraction, using the Shimatzu Co. model XRC-7000 device operating at 40 kV, 20 mA. The test parameters were as follows: 5° to 70° angle, 0.02° step, and 1.2°/min scan speed. The data were analyzed using the Crystallographica Search-Match software from Oxford Cryosystems–United Kingdom (v. 2.1.1.1).

The analysis of OH^- ions was performed by volumetric neutralization titration of an alkaline solution obtained from cement paste solubilization [42,43]. This procedure consisted of diluting 0.50 g of previously milled and hydration-stopped paste in a plastic Erlenmeyer flask containing approximately 200 mL of distilled water for 24 h. The titration process was performed in an aliquot of 50 mL of the initial sample, using 0.1 M hydrochloric acid (HCl) and a blue alcohol solution of bromothymol as a colorimetric indicator, which shows a blue color for basic pH and yellow for acidic pH (turning zone: 7.6 to 6.0). With the volume of acid consumed, the concentration of OH^- (mol/L) and the pH of the studied solution can be estimated through Equations (2) and (3).

$$[OH^-] = \frac{V_{HCl} \times C_{HCl} \times f_c}{V_S} \quad (2)$$

$$pH = -\log\left(\frac{10^{-14}}{[OH^-]}\right) \quad (3)$$

where [OH^-] = the concentration of hydroxyl ions (mmol/L), V_{HCl} = the volume of acid consumed (L), C_{HCl} = the concentration of HCl, f_c = the correction factor, and V_s = the volume of the aliquot used in the titration (L).

3. Results

3.1. Compressive Strength of Concrete Samples

Figure 2 shows the compressive strength results for the concrete samples on the 28th day of hydration.

The different replacements of cement by SF were observed to have statistically influenced the compressive strength of the concrete samples at 28 days through the one-way variance method (ANOVA) with a significance level of 5%. According to Duan et al. [44], SF improves the compressive strength of concrete due to the enhancement of microstructure, since fine particles fill the gaps between cement particles, hydration products, and aggregates, leading to a denser pore structure as well as a denser interfacial transition zone. According to a multiple-variance analysis (the Tukey test), the only statistically different result was the compressive strength of concrete containing 15% SF, with an increase of 37% compared to the control mix.

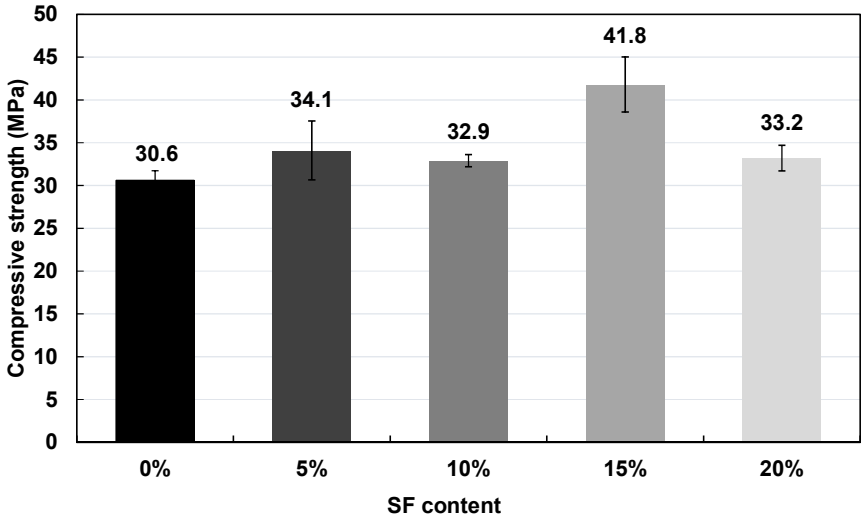

Figure 2. Compressive strength of concrete samples at 28 days.

Behnood and Golafshani [45] stated that the compressive strength of SF concretes increases linearly, varying the SF content from 0 to 30%. However, in this study, the 20% SF content reduced compressive strength by 21% compared to 15% SF. According to Hermann et al. [46], the increase in fine particles that quantitatively exceed the void volume between Portland cement grains promotes the opposite phenomenon of the filler effect, i.e., the spacing of these grains. This spacing effect likely led to reduced particle packing density, compromising the overall compressive strength of the concrete.

Thus, noticeably, there was an optimal point in the cement replacement to maximize the compressive strength of the concrete in the present study at 28 days, namely, the 15% substitution of cement by SF. Some research also showed the optimum content of 15% of SF in cement replacement regarding the compressive strength of concretes at 28 days [47,48]. According to Bhanja and Segunpta [49], the optimum replacement content of SF for 28-day strength is not constant and depends on several factors, such as the w/b ratio, the fineness of SF, and the maximum dimension of aggregates.

3.2. Electrochemical Monitoring Focusing on Passive Film Formation

The electrical resistivity of the concrete mixes was evaluated to assess the potential for steel corrosion. Figure 3 shows the electrical resistivity data over time.

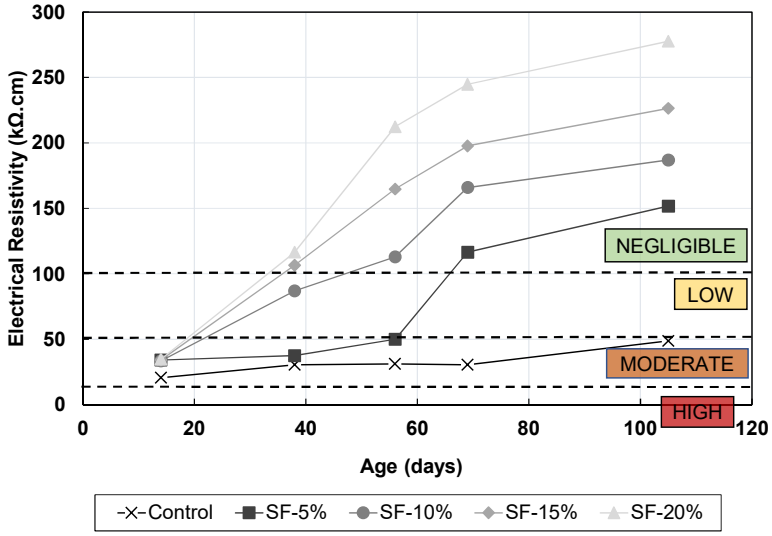

Figure 3. Electrical resistivity of concrete mixes over time for different contents of SF.

All mixes showed increased electrical resistivity over time, since it is related to the degree of hydration of cement and the microstructural change in pore interconnectivity, as observed in other studies [14,50]. Concrete's electrical resistivity increased with the increase in SF content, being more evident the greater the amount of SF. After 105 days of curing, the SF-20% mix presented an electrical resistivity about 5.6 times greater than the control mix, and the mixes containing 5, 10, and 15% of SF showed an increase of 3.1, 3.8, and 4.6 times, respectively.

SF significantly alters the microstructure of concretes, not only through the filler effect, which promotes the densification of the paste, but also by decreasing the critical pore diameter through the deposition of products from pozzolanic reactions [51–53]. Moreover, the reduction in ion concentration in the pore solution, resulting from pozzolanic activity, decreases the mobility of electrons and enhances the resistance against charge transfer, contributing to an increase in electrical resistivity [27].

Considering the corrosion risk classification for concretes produced with Portland cement regarding their electrical resistivity, suggested by Rilem TC 154-EMC [38], concretes with 10, 15, and 20% SF reached the zone where their electrical resistivity was high enough to make corrosion of steel inside the hardened concrete negligible within 30 to 45 days. Concrete samples with 5% cement replacement required more than 60 days to reach an electrical resistivity of 100 kΩ.cm. On the other hand, the control mix took about 100 days to migrate from a moderate to a low probability zone of corrosion and did not achieve the negligible corrosion zone until the end of the study analysis.

The corrosion current density (i_{corr}) is a reliable parameter for monitoring the corrosion mechanism in steel rebar, also indicating passive film formation when stated at a negligible level of corrosion. Figure 4 shows the monitoring data of corrosion current density and the corrosion level indicated according to Andrade and Alonso [38].

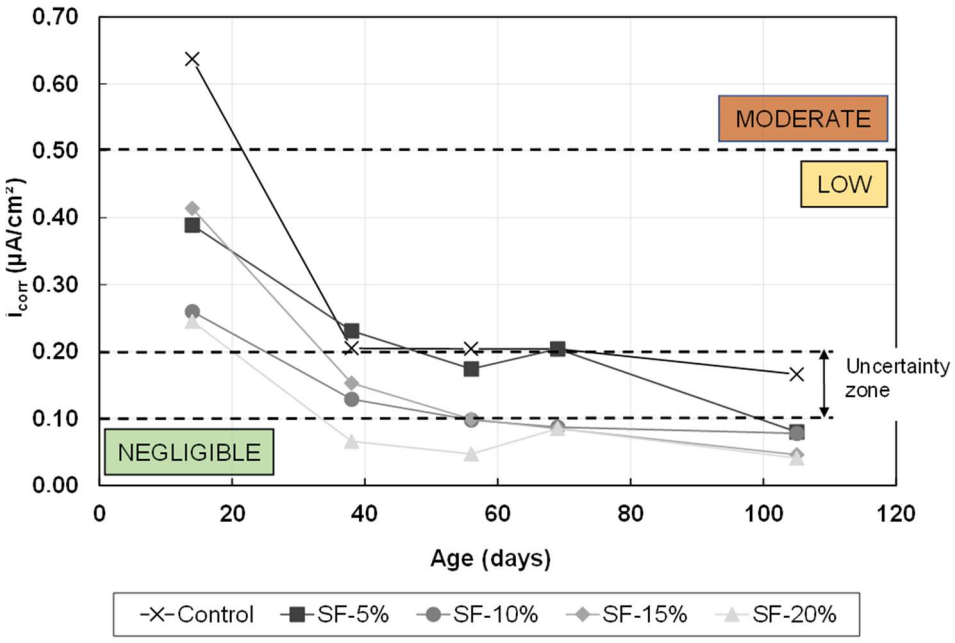

Figure 4. Corrosion current density (i_{corr}) over time for different contents of SF (concrete test).

The control mix presented the higher i_{corr} on the 14th hydration day (0.64 µA/cm^2), placing it within the moderate corrosion zone. On the other hand, all concretes with SF presented low corrosion levels since the first age of analysis, with i_{corr} values equal to 0.39, 0.27, 0.42, and 0.25 µA/cm^2 for mixes containing 5, 10, 15, and 20% of SF, respectively. Over time, all mixes showed a decrease in i_{corr}. The corrosion current density decreased

over time due to the passive film formation on the steel surface, pushed by the increase in electrical resistivity resulting from the progressive cement hydration. At the end of 105 days, samples containing SF showed values below 0.1 μA/cm^2, indicating the formation of a stable passive film.

Considering the passivation limit of 0.1 μA/cm^2, the higher the SF content in concrete, the faster it enters the zone where the corrosion is considered negligible, indicating the formation of passive film on the reinforcement surface. Concrete with 20% SF showed an i_{corr} below 0.1 μA/cm^2 after 30 days, while concrete samples with 10 and 15% SF took about 50 days. Concrete with 5% SF required about 100 days to achieve the same result.

The faster passive film formation on steel inside the concrete samples containing SF was unexpected, since the high alkalinity is essential for its growth, and the pozzolanic reactions are responsible for the consumption of calcium hydroxide, decreasing the pH of the pore solution [10]. Moreover, the higher the amount of SF, the faster the i_{corr} achieved the limit of 0.1 μA/cm^2, indicating faster passive film formation and higher protection against an aggressive environment.

Considering the limit of 0.1 μA/cm^2 as a decision criterion for steel passivation, the control mix did not indicate effective protection against corrosion after 105 days, showing an i_{corr} equal to 0.17 μA/cm^2. However, by increasing the decision criterion to 0.2 μA/cm^2, as some authors have [13,14], passive film formation of the control mix happened on the 38th day of age. It is possible to verify through Figure 5 that, considering the limit of 0.1 μA/cm^2 to indicate the negligible level of corrosion, the passivation time of all samples increased when compared to the limit of 0.2 μA/cm^2.

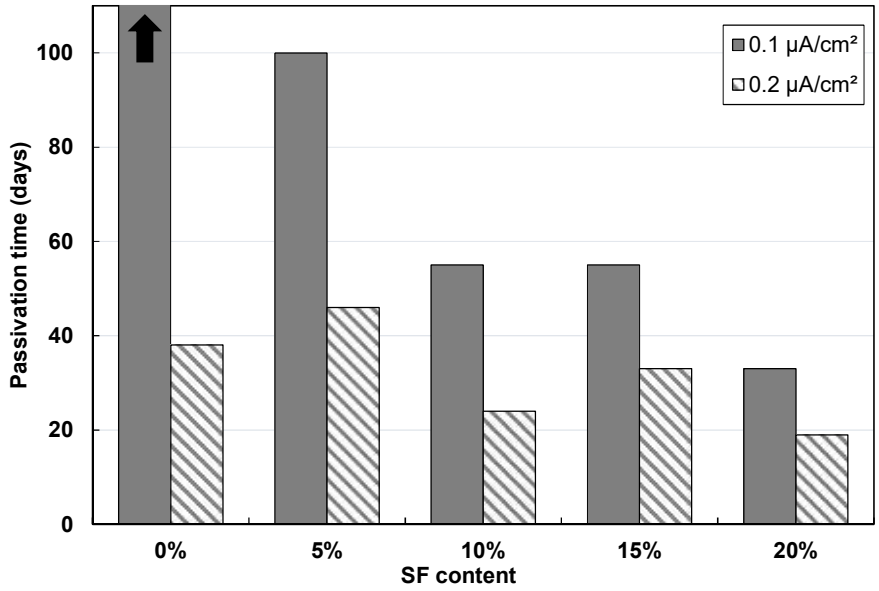

Figure 5. Passivation time for concretes with different contents of SF (concrete test). Note: the arrow at 0% content illustrates that the passivation time was beyond 105 days.

The change in the i_{corr} limit from 0.1 μA/cm^2 to 0.2 μA/cm^2 promoted a decrease in the time required for passive film formation of the mixes containing SF, this being about 57, 52, 36, and 40% lower for mixes with 5, 10, 15, and 20% SF, respectively. In this configuration, it was not possible to observe a tendency of behavior between the samples, and concrete with 20% SF was the one that allowed the faster passive film formation on steel, at the 20th day of age. Following this trend, samples containing 10, 15, and 5% SF presented the following respective times for passivation: 23, 34, and 44 days.

Despite the longer time for evaluation, analyses using the limit of 0.1 μA/cm^2 are more reliable since they provide greater certainty of passive film formation. Also, the data

obtained showed a better tendency regarding the effect of SF content on steel passivation within hardened concrete samples with the limit of 0.1 $\mu A/cm^2$.

Thus, the partial replacement of cement by SF with contents ranging from 5 to 20% improved the protection of steel inside hardened concrete against corrosion. For these mixes, passive film formation occurred earlier than in the control mix, and their electrical resistivity increased, indicating a delayed onset of corrosion due to changes in the physical characteristics of the concrete.

On the other hand, after 105 days, the control mix did not achieve the i_{corr} limit of 0.1 $\mu A/cm^2$ and the negligible zone of risk of corrosion (100 kΩ.cm), indicating that the passive film had not yet stabilized. Therefore, the steel rebar in the control mix concrete was still not protected against corrosion and would require a longer period of electrochemical analysis to ensure passive film formation.

3.3. Monitoring of Hydration Reaction Kinetics

The study also monitored the kinetics of the chemical reactions to understand the influence of pH and the formation of hydration phases on passive film formation. Titration estimated the OH^- ion concentration and pH values of the cement pastes at 28 and 105 days of hydration. Table 6 shows the test results.

Table 6. pH values of cement pastes containing different contents of SF.

MIX	28 Days		105 Days	
	OH^- (mmol/L)	pH	OH^- (mmol/L)	pH
Control mix	17.0	12.2	16.0	12.2
SF-5%	13.8	12.1	12.8	12.1
SF-10%	13.5	12.1	11.4	12.1
SF-15%	10.7	12.0	7.2	11.9
SF-20%	11.1	12.0	6.8	11.8

All mixes presented a pH below 12.6, which is the value cited by Mehta and Monteiro [54] as the minimum limit for steel reinforcement protection against corrosion. The lower pH is responsible for the lower corrosion resistance of the surface film due to the gradual destruction of protective Fe oxides [55]. However, Ai et al. [56] observed that, besides a decline in the passivity of carbon steel with lower alkalinity, passive film formation only failed for pH values under 10.5.

The OH^- concentration and pH of the control mix were the highest values observed at both ages, followed by the mixes with 5%, 10%, 15%, and 20% SF. This behavior is attributed to the reduction in calcium hydroxide due to the pozzolanic activity of SF, along with the reduction in cement content.

Despite the decrease in the alkalinity of the cement pastes over time, the control mix and pastes containing 5 and 10% of SF showed no variation in their pH values. On the other hand, the mixes containing 15 and 20% SF showed a greater reduction in OH^- concentration (33 and 39%, respectively) and a decrease in pH, indicating the higher consumption of calcium hydroxide from pozzolanic activity. However, this reduction did not promote any negative effect on the passive film formation of steel inside the hardened concrete.

Havdahl and Justnes [57] stated that, despite the complete depletion of CH (portlandite) in cement pastes with 15 and 20% SF, the pH in their pore solution remained high enough for passive film formation due to a lesser amount of alkali silicates or the adsorption of Na^+ and K^+ by silanol groups, resulting in an alkaline C-S-H composition. In the present study, the slight decrease in pH due to the incorporation of SF in concrete samples did not reach the limit of 10.5 stated by Ai et al. [56] for passive film formation. Also, it provided

an environment with reduced ionic strength (referring to the concentration of ions in the environment), which is better for passive film formation [14,55].

The correlation between the pH values and SF contents of the cement pastes resulted in a linear behavior on the 28th and 105th day, with an R^2 coefficient of 0.951 (Figure 6A) and 0.888 (Figure 6B), respectively. Therefore, the higher the SF content, the greater the reduction in clinker and the higher the pozzolanic activity, resulting in a higher reduction in pH values in cementitious materials.

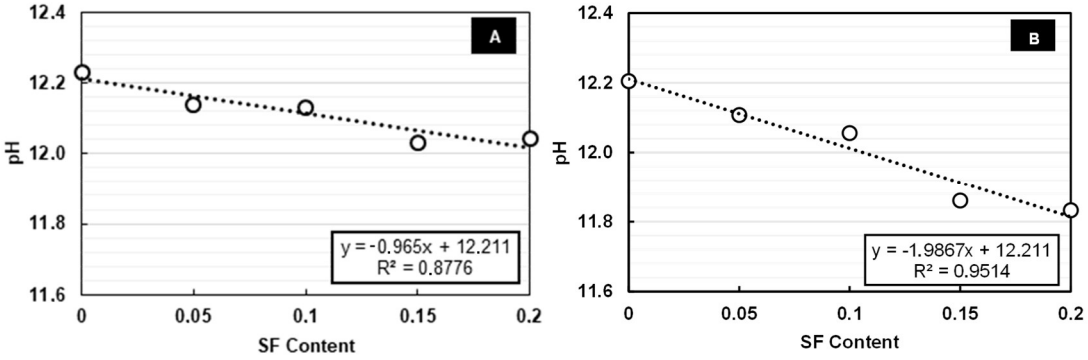

Figure 6. Correlation between pH and SF content at (**A**) day 28 and (**B**) day 105.

Cement hydration products were investigated by the X-ray diffraction technique (XRD). Figure 7 shows the patterns obtained for cement paste samples at 28 days.

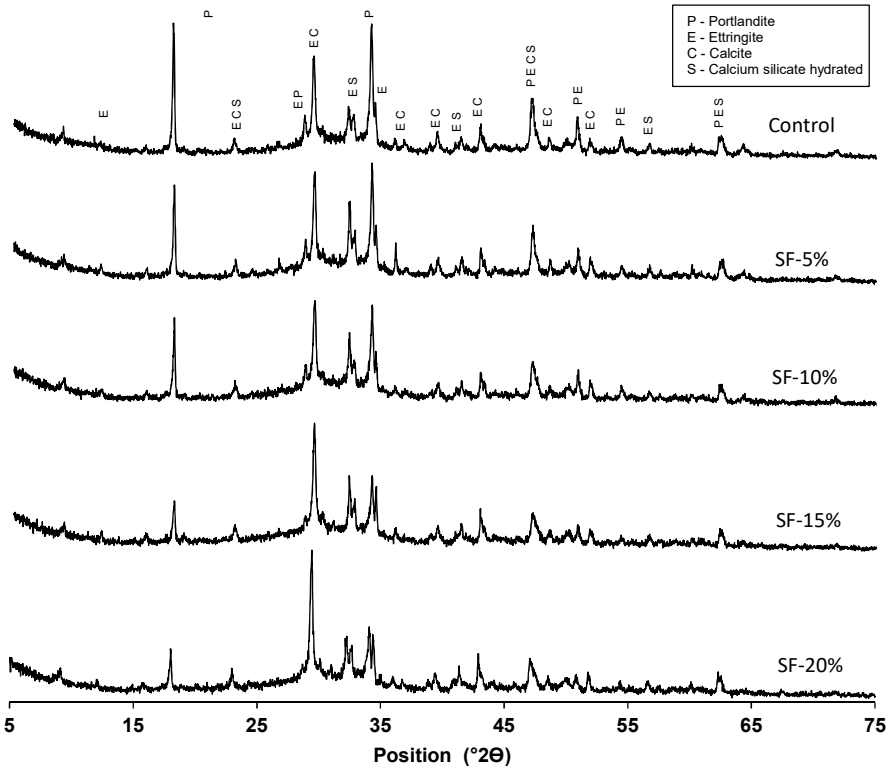

Figure 7. X-ray diffraction of cement paste samples after 28 days of hydration.

The XRD results indicated the presence of several phases from hydration of cement, such as portlandite ($Ca(OH)_2$), calcite ($CaCO_3$), ettringite ($Ca_6A_{l2}(SO_4)_3(OH)_{12}.26H_2O$), and calcium silicate (C-S-H). Although XRD does not allow for precise quantitative analysis, the authors performed a semi-quantitative evaluation to estimate the influence of different

SF contents on these phases. This approach aimed to provide insight into phase variations due to SF content, acknowledging the limitations of XRD for accurate quantification.

The pozzolanic activity leads to the consumption of available portlandite in the cement matrix and the formation of secondary C-S-H. To analyze the remaining portlandite content, a comparison was made between one of its main peaks (2θ = 17.96°) across different samples. Figure 8 shows the partial diffractograms at 28 days, highlighting the region of the portlandite peak.

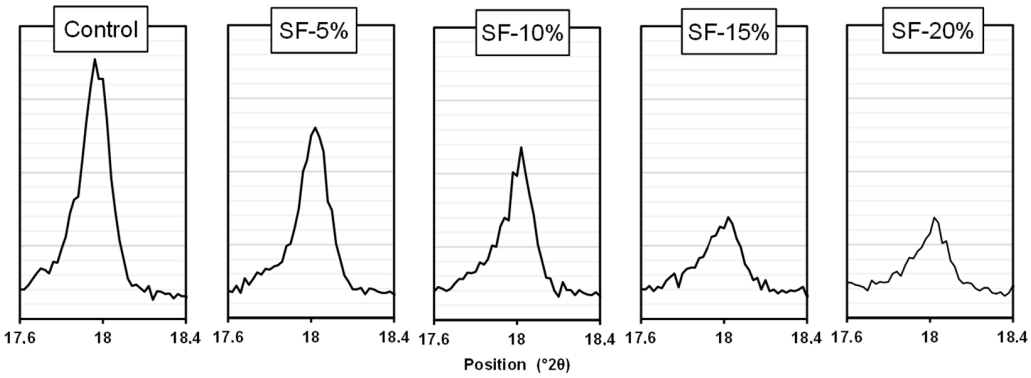

Figure 8. Partial diffractograms of cement pastes at 28 days, with emphasis on the region of the portlandite peak (2θ = 17.96°).

The partial diffractograms showed a decrease in the peak of portlandite in the SF-containing mixes compared to the control mix. The portlandite peak counts decreased from 710 in the control mix to 520, 472, 278, and 274 in the pastes containing 5, 10, 15 and 20% SF, respectively. Similarly, Gómez-Zamorano, Garcia-Guillén, and Acevedo-Dávila [58] verified a decrease in the amount of portlandite with an increase in SF content through qualitative analysis of the intensity of peaks present in XRD results. The reduction in the portlandite peak became more pronounced with a higher SF content, a behavior promoted by the decrease in clinker amount and hydroxide consumption due to the pozzolanic reactions.

Figures 9 and 10 show, respectively, the XRD patterns obtained for paste samples at 105 days and the partial diffractograms for the portlandite peak.

At 105 days of hydration, the control mix showed an increase of 10% in the intensity of portlandite peak when compared to the results at 28 days, indicating the continuous hydration of cement over time. On the other hand, the mixes containing 5, 10, 15, and 20% SF showed a more substantial decrease in portlandite peak intensity than the one observed at 28 days, equal to 33.3, 46.1, 69.2, and 70.5%, respectively. According to Abo-El-Enein et al. [59] and Dotto et al. [60], portlandite peak intensity decreases progressively with the hydration time in mixes containing SF due to the continuous consumption of portlandite by pozzolanic reactions. Yogendran, Langan, and Ward [61] found that portlandite content decreases as SF content increases, with complete consumption in pastes containing 15% SF and 20% SF.

The accuracy of the qualitative analysis was investigated by correlating the intensity of the portlandite peak with the hydroxyl ion concentration in cement pastes. Figure 11 illustrates this correlation.

A linear correlation with a strong coefficient (R^2 = 0.8525) was obtained between the intensity peak of portlandite in the XRD patterns and the hydroxyl ion (OH^-) concentration of the cement pastes, indicating the XRD accuracy quantitatively. Therefore, the qualitative analysis of the portlandite peak in XRD patterns reflects the alkalinity of hardened cement pastes and, thus, can assist in evaluating the environment for passive film formation.

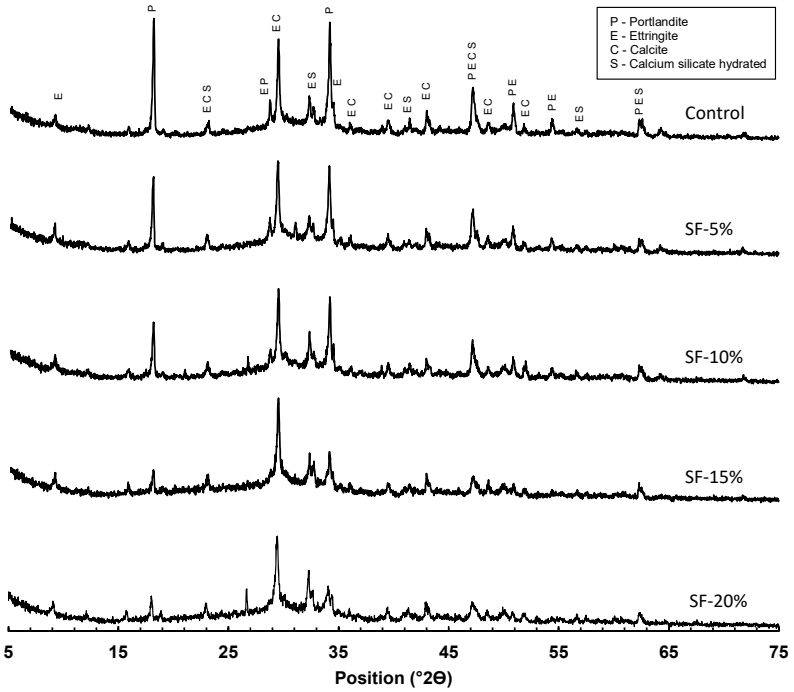

Figure 9. X-ray diffraction of cement paste samples after 105 days of hydration.

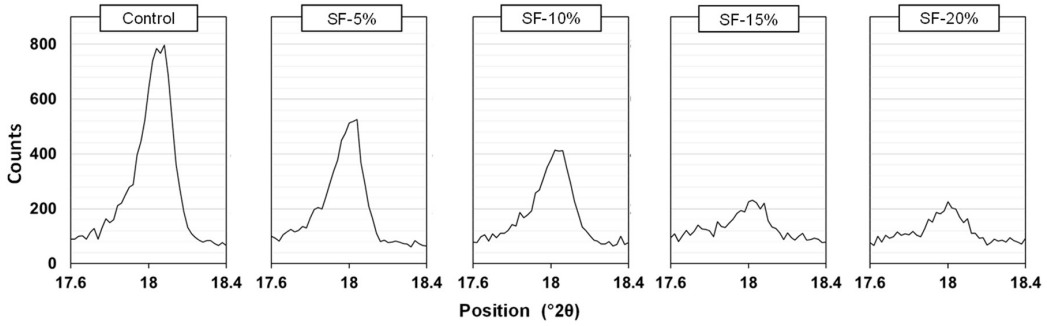

Figure 10. Partial diffractograms of the series at 105 days, with emphasis on the location region of the portlandite peak.

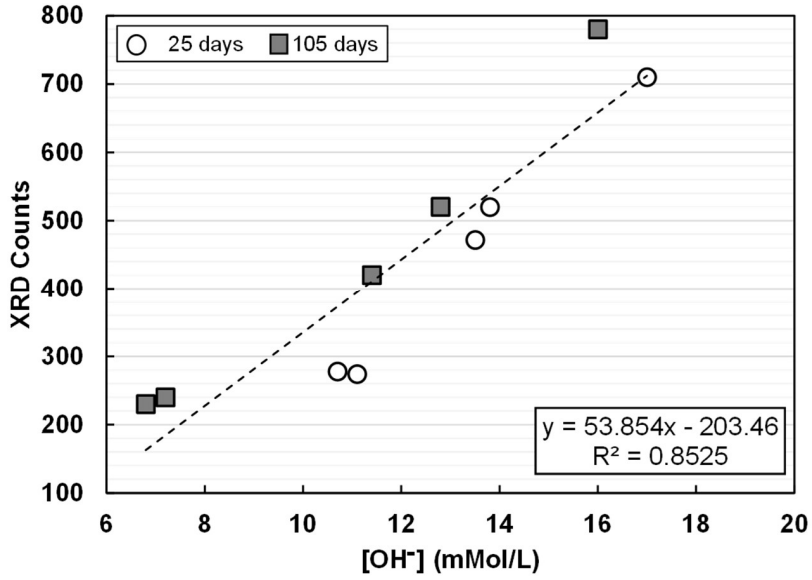

Figure 11. Correlation between intensity of the peak of portlandite and hydroxyl ion (OH^-) concentration by titration of cement pastes.

3.4. The Relation Between CH Content, pH, Electrical Resistivity, and i_{corr}

The portlandite contents, obtained through qualitative analysis of the peaks of CH in the XRD patterns, along with the pH values of the cement pastes, were used to assess their relation to the electrical resistivity of the corresponding concrete mixes after 105 days of hydration. As shown in Figure 12A,B, the comparison of the qualitative analysis of CH content through XRD and pH with electrical resistivity presented correlation coefficients of 0.96 and 0.85, respectively.

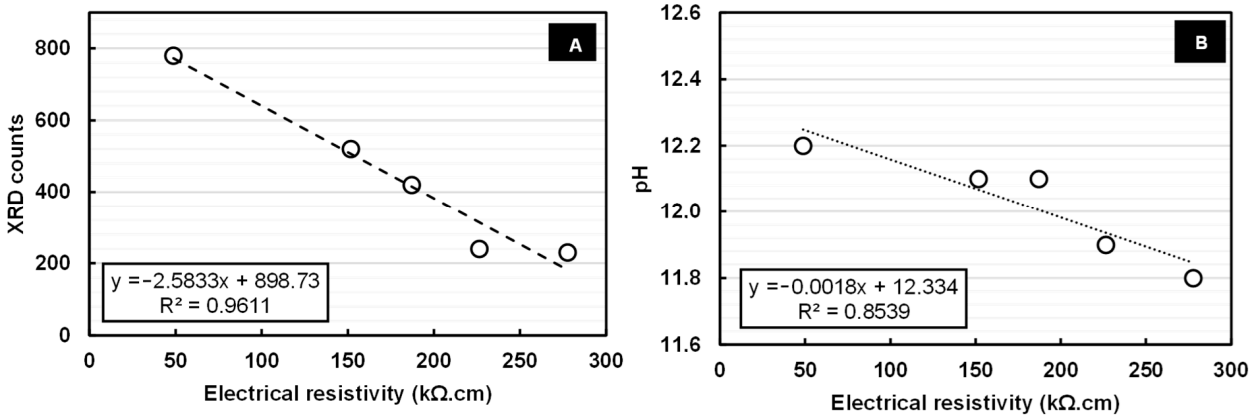

Figure 12. Correlation of electrical resistivity of concrete samples with (**A**) XRD counts and (**B**) pH values of cement pastes after 105 days of hydration.

Cruz et al. [62] and Ghoddousi and Saadabadi [63] also found good correlation coefficients between electrical resistivity and CH content in Portland cement mortars and concretes, the latter being directly related to the pH value, since CH is the main font of hydroxyl ions in the cement matrix. The reduction in CH content and pH was shown through XRD patterns and titration, promoted an increase in electrical resistivity, and resulted in linear trends with high correlation coefficients (R^2), indicating that it occurred due to the reduction in the amount of ions and their mobility, as stated by Page and Vernnesland [64].

Figure 13A,B presents a comparison between the qualitative analysis of CH content as determined through XRD and pH with i_{corr}.

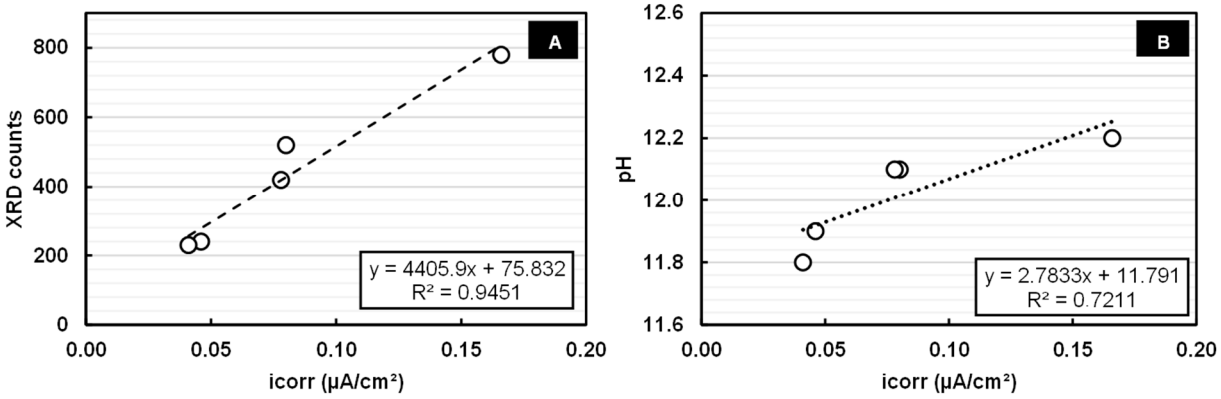

Figure 13. Correlation between i_{corr} values of concrete samples and (**A**) XRD counts and (**B**) pH values of cement pastes after 105 days of hydration.

The CH content and pH value were parameters directly proportional to the i_{corr} of steel inside the hardened concrete after 105 days of hydration, showing good adherence with a linear regression (R^2 = 0.94 and R^2 = 0.72, respectively). Thus, a higher content

of CH and elevated pH values in the cement matrix promoted a greater i_{corr} and lower polarization resistance, indicating the greater instability of the passive film.

According to Mancio et al. [55], the polarization resistance of carbon steel decreases when the pH of the environment is reduced from 13 to 11 and then presents a strong decline, since the ionic strength of the medium is kept constant. However, the ionic strength in hardened concrete is not constant due to the continuous hydration of cement and CH consumption by pozzolanic reactions when SF is part of the binder. Thus, polarization resistance should increase and i_{corr} decrease with a pH varying from 13 to 11 [55], as observed in the present study. Ortolan, Mancio, and Tutikian [14] verified that the reduction in pH, caused by the partial substitution of cement for SF, increased the polarization resistance of steel rebar within hardened concrete and, consequently, resulted in lower i_{corr} values during 91 days of hydration.

Based on the correlation coefficients obtained for both electrochemical parameters, CH content and pH were considered dependent parameters for the electrical resistivity and the i_{corr}. Thus, it is expected that the qualitative analysis of XRD and pH will be useful for predicting passive film formation. This can be achieved by classifying electrical resistivity according to the steel rebar risk of corrosion and i_{corr} according to the level of corrosion onset.

4. Conclusions

This study investigated the effects of partially replacing cement with silica fume in concrete mixtures. The emphasis was on the durability of steel reinforcement, considering parameters such as the electrical resistivity, corrosion current density (i_{corr}), portlandite content, and pH of cement pastes. The main conclusions are summarized below:

- The 15% content of SF is an optimum content regarding the compressive strength of concretes at 28 days, being 36.6% higher than that of the control mix;
- The formation of passive film on steel inside hardened concrete is not instantaneous, taking from twenty days to several weeks for its complete protection against corrosion;
- Analyses using the 0.1 $\mu A/cm^2$ limit are more reliable since they provide a greater certainty of passive film formation;
- The corrosion current density of the control mix did not reach the limit of a negligible level of corrosion (0.1 $\mu A/cm^2$) until 105 days of curing, indicating susceptibility to steel corrosion;
- Despite the considerable consumption of portlandite, verified through qualitative analysis via XRD, the partial replacement of cement by SF, with contents ranging from 5 to 20%, provided an improvement in concrete performance regarding the formation of passive film;
- The formation of passive film on steel surfaces was faster the higher the SF content;
- The qualitative analysis of XRD patterns was efficient in evaluating the compounds formed and consumed during hydration, indicating the alkalinity of cement pastes and the evolution of pozzolanic reactions;
- The CH content and pH could be useful for predicting passive film formation, since they provided a good correlation coefficient with electrical resistivity and i_{corr} values after 105 days of hydration;
- After 105 days of hydration, the lower pH contributed to passive film formation on the steel surface, since i_{corr} values for steel decreased with the pH reduction from 12.2 to 11.8.

It is important to note that, although electrochemical techniques allow an initial assessment of the corrosion risk, the direct correlation between i_{corr} and the effective steel mass loss is not always linear. Future studies should seek to establish better relationships

between electrochemical tests and empirical data. This approach will contribute to a better understanding of the effects of different SF contents on long-term corrosion, widening the applicability of electrochemical techniques.

Author Contributions: Conceptualization, M.A., I.A.O., D.H.d.B., G.C.R., G.M., and M.H.F.d.M.; Data curation, M.A., I.A.O., D.H.d.B., G.C.R., G.M., and M.M.F.; Formal analysis, M.A., I.A.O., D.H.d.B., G.C.R., and G.M.; Methodology, M.A., I.A.O., D.H.d.B., G.C.R., and G.M.; Supervision, M.H.F.d.M.; Writing—original draft, M.A., I.A.O., D.H.d.B., G.C.R., and G.M.; Writing—review and editing, M.M.F. and M.H.F.d.M. All authors have read and agreed to the published version of the manuscript.

Funding: This research was funded by the Araucaria Foundation, the Brazilian National Council for Scientific and Technological Development (CNPq), and the Brazilian Federal Agency for Support and Evaluation of Graduate Education (CAPES).

Data Availability Statement: The original contributions presented in this study are included in the article. Further inquiries can be directed to the corresponding author.

Acknowledgments: The authors would like to thank the following institutions: the Materials and Structures Laboratory of the Department of Civil Construction of UFPR (LAME); the Post-graduate Program in Civil Engineering (PPGEC) and the Center for Studies in Civil Engineering (CESEC), both at UFPR, for partial support; the UFPR Multi-user Diffraction X-ray Laboratory for assistance with the use of equipment purchased through FINEP CT-INFRA 793/2004 and 3080/2011 projects. In addition, the authors would like to thank the Academic Publishing Advisory Center of the Federal University of Paraná (UFPR) for their assistance with translation and proofreading.

Conflicts of Interest: The authors declare no conflicts of interest.

References

1. de Medeiros, M.H.F.; Gobbi, A.; Groenwold, J.; Marcondes, C.G.; Helene, P. High strength reinforced concrete with metakaolin and silica fume in marine environment: An experimental work. *Hormigón Y Acero* **2012**, *63*, 57–66.
2. Pradhan, D. Corrosion behaviour of steel reinforcement in concrete exposed to composite chloride-sulfate environment. *Constr. Build. Mater.* **2014**, *72*, 398–410. [CrossRef]
3. Dogan, M. Corrosion failure in concrete reinforcement to damage during seismic. *Eng. Fail. Anal.* **2015**, *56*, 275–287. [CrossRef]
4. Milić, P.; Marić, M.K. Climate change effect on durability of bridges and other infrastructure. *Građevinar* **2023**, *75*, 896–906. [CrossRef]
5. Amleh, L.; Hassan, M.; Hussein, L. Influence of Climate Change on the Probability of Chloride-Induced Corrosion Initiation for RC Bridge Decks Made of Geopolymer Concrete. *Sustainability* **2024**, *16*, 8200. [CrossRef]
6. Inam, I.; Sediqmal, M.; Hesam, A.M. The Impact of Climate Change and Carbonation on the Durability of Concrete Structures in Afghanistan. *Nangarhar Univ. Int. J. Biosci.* **2024**, *3*, 282–285. [CrossRef]
7. Hussain, R.R.; Alhozaimy, A.; Al-Negheimish, A.; Al-Zaid, R.; Singh, D.D.N. Mechanism of nucleation and growth of passive film on steel reinforcing bar at different durations of its exposure in concrete pore solution at nanoscale. *ACI Mater. J.* **2015**, *112*, 523–534. [CrossRef]
8. Dormohammadi, H.; Pang, Q.; Murkute, P.; Árnadóttir, L.; Isgor, O.B. Investigation of iron passivity in highly alkaline media using reactive-force field molecular dynamics. *Corros. Sci.* **2019**, *157*, 31–40. [CrossRef]
9. Mudra, S.; Criado, M.; Bernal, S.A.; Provis, J.L. Chloride-induced corrosion of steel rebars in simulated pore solutions of alkali-activated concretes. *Cem. Concr. Res.* **2017**, *100*, 385–397. [CrossRef]
10. Williamson, J.; Isgor, O.B. The effect of simulated concrete pore solution composition and chlorides on the electronic properties of passive films on carbon steel rebar. *Corros. Sci.* **2016**, *106*, 82–95. [CrossRef]
11. Sun, X.H.; Zuo, X.B.; Win, G.J.; Jiang, K.; Tang, Y.J. Eletrochemical and microscopic investigation on passive behaviour of ductile iron in simulated cement-mortar pore solution. *Constr. Build. Mater.* **2017**, *150*, 703–713. [CrossRef]
12. Ai, Z.; Jiang, J.; Sun, W.; Jiang, X.; Yu, B.; Wang, K.; Zhang, Z.; Song, D.; Ma, H.; Zhang, J. Enhanced passivation of alloy corrosion-resistant steel Cr10Mo1 under carbonation—Passive film formation, the kinetics and mechanism analysis. *Cem. Concr. Compos.* **2018**, *92*, 178–187. [CrossRef]
13. Poursaee, A.; Hansson, C.M. Reinforcing steel passivation in mortar and pore solution. *Cem. Concr. Res.* **2007**, *37*, 1127–1133. [CrossRef]

14. Ortolan, V.K.; Mancio, M.; Tutikian, B.F. Evaluation of the influence of the pH of concrete pore solution on the corrosion resistance of steel reinforcement. *J. Build. Pathol. Rehabil.* **2016**, *1*, 10. [CrossRef]
15. Liu, M.; Cheng, X.; Li, X.; Pan, Y.; Li, J. Effect of Cr on the passive film formation mechanism of steel rebar in saturated calcium hydroxide solution. *Appl. Surf. Sci.* **2016**, *389*, 1182–1191. [CrossRef]
16. Volpi, E.; Olietti, A.; Stefanoni, M.; Trasatti, S.P. Electrochemical characterization of mild steel in alkaline solutions simulating concrete environment. *J. Electroanal. Chem.* **2015**, *736*, 38–46. [CrossRef]
17. Shi, J.; Ming, J.; Sun, W. Passivation and chloride-induced corrosion of a duplex alloy steel in alkali-activated slag extract solutions. *Constr. Build. Mater.* **2017**, *155*, 992–1002. [CrossRef]
18. Elsener, B.; Rossi, A. Passivation of Steel and Stainless Steel in Alkaline Media Simulating Concrete. In *Encyclopedia of Interfacial Chemistry*; Elsevier: Oxford, UK, 2018; pp. 365–375. [CrossRef]
19. Peng, Y.; Liu, L.; Wang, S.; Lin, Y.; Sun, Y.; Xia, R. Effect of simulated pore solution on passivation characteristic of P110 steel. *J. Pet. Sci. Eng.* **2018**, *167*, 949–956. [CrossRef]
20. Koga, G.Y.; Albert, B.; Roche, V.; Nogueira, R.P. On the intrinsic passivating ability of Belite-Ye'elimite-Ferrite towards carbon steel: A straightforward comparison with ordinary Portland cement. *Corros. Sci.* **2019**, *147*, 141–151. [CrossRef]
21. Munot, H.; Deshpande, P.; Modhera, C. Electrochemical investigations on semi-conducting properties of a passive film on conducting polypyrrole coated low carbon steel in a simulated concrete pore solution. *Port. Electrochim. Acta* **2019**, *37*, 43–50. [CrossRef]
22. Gromboni, M.F.; Sales, A.; de AM Rezende, M.; Moretti, J.P.; Corradini, P.G.; Mascaro, L.H. Impact of agro-industrial waste on steel corrosion susceptibility in media simulating concrete pore solutions. *J. Clean. Prod.* **2021**, *284*, 124697. [CrossRef]
23. Zhang, Z.; Yu, X.; Gong, N.; Zhang, Y.; Wu, H.; Mao, X.; Niu, G. Passivation Behavior of Cr-Modified Rebar in Simulated Concrete Pore Solutions with Different pH. *J. Mater. Res. Technol.* **2023**, *26*, 246–259. [CrossRef]
24. Liu, G.; Zhang, P.; Liu, C.; Zhang, Y. Influence of pH on Passivation of Mild Steel in Simulated Concrete Pore Solution: Electrochemical, ToF-SIMS and ReaxFF Study. *Dev. Built Environ.* **2024**, *19*, 100502. [CrossRef]
25. Alhozaimy, A.; Hussain, R.R.; Al-Negheimish, A. Significance of oxygen concentration on the quality of passive film formation for steel reinforced concrete structures during the initial curing of concrete. *Cem. Concr. Compos.* **2016**, *65*, 171–176. [CrossRef]
26. Fan, L.; Meng, W.; Teng, L.; Khayat, K.H. Effects of lightweight sand and steel fiber contents on the corrosion performance of steel rebar embedded in UHPC. *Constr. Build. Mater.* **2020**, *238*, 117709. [CrossRef]
27. Sobhani, J.; Najimi, M. Electrochemical impedance behavior and transport properties of silica fume contained concrete. *Constr. Build. Mater.* **2013**, *47*, 910–918. [CrossRef]
28. Ashraf, M.; Iqbal, M.F.; Rauf, M.; Ashraf, M.U.; Ulhaq, A.; Muhammad, H.; Liu, Q. Developing a sustainable concrete incorporating bentonite clay and silica fume: Mechanical and durability performance. *J. Clean. Prod.* **2022**, *337*, 130315. [CrossRef]
29. de Medeiros, M.H.F.; Raisdorfer, J.W.; Filho, J.H. Influência da sílica ativa e do metacaulim na velocidade de carbonatação do concreto: Relação com resistência, absorção e relação a/c. Ambient. *Construído* **2017**, *17*, 125–139. [CrossRef]
30. De Oliveira, A.M.; Cascudo, O. Effect of mineral additions incorporated in concrete on thermodynamic and kinetic parameters of chloride-induced reinforcement corrosion. *Constr. Build. Mater.* **2018**, *192*, 467–477. [CrossRef]
31. *C150/150M-24*; Standard Specification for Portland Cement. ASTM International: Detroit, MI, USA, 2019. [CrossRef]
32. *NBR 15895*; Materiais Pozolânicos—Determinação do Teor de Hidróxido de Cálcio Fixado—Método Chapelle Modificado. Associação Brasileira de Normas Técnicas—ABNT: Rio de Janeiro, Brazil, 2010.
33. Raverdy, M.; Brivot, F.; Paillere, M.A.; Dron, R. Appreciation of Pozzolanic Reactivity of Minor Components. In *7th International Congress Chemical Cement*; The Congress : Paris, France, 1980.
34. *NBR 7480*; Barras e Fios de Aço Destinados a Armaduras Para Concreto Armado. Associação Brasileira de Normas Técnicas—ABNT: Rio de Janeiro, Brazil, 2007.
35. *NBR 5739*; Concreto—Ensaio de Compressão de Corpos de Prova Cilíndricos. Associação Brasileira de Normas Técnicas—ABNT: Rio de Janeiro, Brazil, 2018.
36. Neithalath, N.; Persun, J.; Hossain, A. Hydration in high-performance cementitious systems containing vitreous calcium aluminosilicate or silica fume. *Cem. Concr. Res.* **2009**, *39*, 473–481. [CrossRef]
37. Filho, J.H.; Rodrigues, C.S.; Ribeiro, L.S.O.P.; Medeiros, M.H.F. Evaluation of sample drying methods to determine the apparent porosity and estimation of degree of hydration of portland cement pastes. *J. Build. Pathol. Rehabil.* **2021**, *6*, 1. [CrossRef]
38. Andrade, C.; Alonso, C. Recommendations of RILEM TC 154-EMC: Test methods for on-site corrosion rate measurement of steel reinforcement in concrete by means of the polarization resistance method. *Mater. Struct.* **2004**, *37*, 623–643. [CrossRef]
39. Goñi, S.; Andrade, C. Synthetic concrete pore solution chemistry and rebar. *Cem. Concr. Res.* **1990**, *20*, 525–539. [CrossRef]
40. Gonzalez, J.A.; Feliu, S.; Rodrigues, P.; Ramirez, E.; Alonso, C.; Andrade, C. Some questions on the corrosion of steel in concrete—Part 1: When, how and how much steel corrodes. *Mater. Strcutures* **1996**, *29*, 40. [CrossRef]
41. Song, G. Theoretical analysis of the measurement of polarisation resistance in reinforced concrete. *Cem. Concr. Compos.* **2000**, *22*, 407–415. [CrossRef]

42. Filho, J.H.; Gobbi, A.; Pereira, E.; Tanaka, R.S.; Medeiros, M.H.F. Atividade pozolânica de adições minerais para cimento Portland (Parte I): Índice de atividade pozolânica com cimento cal (IAP), difração de raios-x (DRX) e Chapelle modificado. *Rev. Mater.* **2017**, *22*, e11872. [CrossRef]
43. Filho, J.H.; Gobbi, A.; Pereira, E.; Tanaka, R.S.; Medeiros, M.H.F. Atividade pozolânica de adições minerais para cimento Portland (Parte II): Índice de atividade pozolânica com cimento Portland (IAP), difração de raios-X (DRX) e termogravimetria (TG/DTG). *Rev. Mater.* **2017**, *22*, e11873. [CrossRef]
44. Duan, P.; Shui, Z.; Chen, W.; Shen, C. Efficiency of mineral admixtures in concrete: Microstructure, compressive strength and stability of hydrate phases. *Appl. Clay Sci.* **2013**, *83–84*, 115–121. [CrossRef]
45. Behnood, A.; Golafshani, E.M. Predicting the compressive strength of silica fume concrete using hybrid artificial neural network with multi-objective grey wolves. *J. Clean. Prod.* **2018**, *202*, 54–64. [CrossRef]
46. Hermann, A.; Langaro, E.A.; Silva, S.H.L.D.A.; Klein, N.S. Particle packing of cement and silica fume in pastes using an analytical model. *Rev. IBRACON Estrut. E Mater.* **2016**, *9*, 48–65. [CrossRef]
47. Johari, M.A.M.; Brooks, J.J.; Kabir, S.; Rivard, P. Influence of supplementary cementitious materials on engineering properties of high strength concrete. *Constr. Build. Mater.* **2011**, *25*, 2639–2648. [CrossRef]
48. Mohamed, H.A. Effect of fly ash and silica fume on compressive strength of self-compacting concrete under different curing conditions. *Ain Shams Eng. J.* **2011**, *2*, 79–86. [CrossRef]
49. Bhanja, S.; Sengupta, B. Optimum Silica Fume Content and Its Mode of Action on Concrete. *ACI Mater. J.* **2003**, *100*, 407–412.
50. Madani, H.; Bagheri, A.; Parhizkar, T.; Raisghasemi, A. Chloride penetration and electrical resistivity of concretes containing nanosilica hydrosols with different specific surface areas. *Cem. Concr. Compos.* **2014**, *53*, 18–24. [CrossRef]
51. Bagheri, A.R.; Zanganeh, H.; Moalemi, M.M. Mechanical and durability properties of ternary concretes containing silica fume and low reactivity blast furnace slag. *Cem. Concr. Compos.* **2012**, *34*, 663–670. [CrossRef]
52. Khodabakhshian, A.; Ghalehnovi, M.; de Brito, J.; Shamsabadi, E.A. Durability performance of structural concrete containing silica fume and marble industry waste powder. *J. Clean. Prod.* **2018**, *170*, 42–60. [CrossRef]
53. Sadrmomtazi, A.; Tahmouresi, B.; Saradar, A. Effects of silica fume on mechanical strength and microstructure of basalt fiber reinforced cementitious composites (BFRCC). *Constr. Build. Mater.* **2018**, *162*, 321–333. [CrossRef]
54. Mehta, P.K.; Monteiro, P.J.M. *Concreto: Estrutura; Propriedades e Materiais*; Ibracon: Sao Paulo, Brazil, 2014.
55. Mancio, M.; Kusinski, G.; Monteiro, P.J.M.; Devine, T.M. Electrochemical and in-situ SERS study of passive film characteristics and corrosion performance of 9% Cr microcomposite steel in highly alkaline environments. *J. ASTM Int.* **2009**, *6*, 1–10. [CrossRef]
56. Ai, Z.; Jiang, J.; Sun, W.; Song, D.; Ma, H.; Zhang, J.; Wang, D. Passive behaviour of alloy corrosion-resistant steel Cr10Mo1 in simulating concrete pore solutions with different pH. *Appl. Surf. Sci.* **2016**, *389*, 1126–1136. [CrossRef]
57. Havdahl, J.; Justnes, H. Tiie alkalinity of cbmentitious pastes with microsilica cured at ambient and, Nord. *Concr. Res. Publ.* **1993**, *12*, 42–56.
58. Gómez, Z.L.Y.; Garcia, G.G.; Acevedo, D.J.L.; Gómez-Zamorano, L.Y.; Gárcia-Guillén, G.; Acevedo-Dávila, J.L. Estudo da hidratação de pastas de cimento Portland com substituições de escória granulada de alto forno, cinza volante e metacaulim: Efeito da utilização de dois aditivos superplastificantes. *Alconpat* **2015**, *5*, 203–218. Available online: https://www.scielo.org.mx/scielo.php?pid=S2007-68352015000300203&script=sci_arttext&tlng=pt (accessed on 4 December 2024).
59. Abo-El-Enein, S.A.; El-kady, G.; El-Sokkary, T.M.; Gharieb, M. Physico-mechanical properties of composite cement pastes containing silica fume and fly ash. *HBRC J.* **2015**, *11*, 7–15. [CrossRef]
60. Dotto, J.M.R.R.; De Abreu, A.G.; Molin, D.C.C.C.D.; Müller, I.L. Influence of silica fume addition on concretes physical properties and on corrosion behaviour of reinforcement bars. *Cem. Concr. Compos.* **2004**, *26*, 31–39. [CrossRef]
61. Yogendran, V.; Langan, B.W.; Ward, M.A. Hydration of cement and silica fume paste. *Cem. Concr. Res.* **1991**, *21*, 691–708. [CrossRef]
62. Cruz, J.M.; Fita, I.C.; Soriano, L.; Payá, J.; Borrachero, M.V. The use of electrical impedance spectroscopy for monitoring the hydration products of Portland cement mortars with high percentage of pozzolans. *Cem. Concr. Res.* **2013**, *50*, 51–61. [CrossRef]
63. Ghoddousi, L.; Adelzade, S. Study on hydration products by electrical resistivity for self-compacting concrete with silica fume and metakaolin. *Constr. Build. Mater.* **2017**, *154*, 219–228. [CrossRef]
64. Page, C.L. Vennesland, Pore solution composition and chloride binding capacity of silica-fume cement pastes. *Matériaux Constr.* **1983**, *16*, 19–25. [CrossRef]